Journal of Materials Chemistry

Cite this: J. Mater. Chem., 2012, 22, 3069

www.rsc.org/materials

PAPER

Thermodynamic-effect-induced growth, optical modulation and UV lasing of hierarchical ZnO Fabry–Pérot resonators

Hongxing Dong,[ab] Shulin Sun,[c] Liaoxin Sun,[d] Weihang Zhou,[b] Lei Zhou,[b] Xuechu Shen,[b] Zhanghai Chen,*[b] Jun Wang[a] and Long Zhang*[a]

Received 2nd September 2011, Accepted 15th November 2011
DOI: 10.1039/c1jm14330a

High quality ZnO multilayer hexagonal microplates and microtubes were fabricated *via* a simple carbothermal method without any catalysts, carrier gases, or low pressure. The formation of the ZnO microstructures with different morphologies was discussed in detail, and a possible thermodynamic viewpoint was proposed. Fabry–Pérot (FP) modes and UV lasing were directly observed using a spatially resolved spectroscopic technique. All the resonant modes observed experimentally were identified using finite-difference-time-domain simulations. Excitation power and temperature dependence of lasing properties of the ZnO microplate were further studied. Compared with the conventional one-dimensional nanowire/nanobelt FP cavities, such ZnO multilayer vertical-FP resonators have much less optical loss and excellent optical responses and may find potential applications in UV microlasers.

Introduction

Crystalline microstructures of regular shape as optical microcavities have been attracting great interest due to their potential applications in optical devices.[1–3] The microstructure itself functions as both the gain medium and the optical resonator. Light propagation can be well confined and modulated in all three dimensions. This precise control of the light–matter interaction is important for both fundamental studies on quantum electrodynamics and the development of miniature optical devices. The Fabry–Pérot (FP) microcavities, as one of the most important types of optical cavities, have been successfully achieved in many microstructures such as ZnO nanowires/nanobelts,[4,5] GaN nanowires,[6] CdS nanowires,[7] InP nanowires,[8] and organic nanowires.[9] The ends of the one dimensional (1D) nanowire function as two reflecting mirrors. Despite tremendous progress that has been made in the last decade, there are two major drawbacks that cannot be avoided.[10] In most of the previous studies, nanowires or nanobelts need to be removed from their native growth substrate and transferred onto a clean silicon or quartz slide by means of ultrasonic or mechanical techniques, resulting in a non-negligible damage of the cavities and hence an increase in optical losses. On the other hand, in general, the nanowires and nanobelts are in direct contact with the substrates along their entire length, resulting in high optical losses as well. Therefore, an interesting and challenging issue is to develop new and efficient FP microcavities.

Zinc oxide (ZnO), an exceptionally important semiconductor with a direct wide band gap (3.37 eV) and large exciton binding energy (60 meV) at room temperature, is one of the most attractive materials for photonic applications in the visible and near UV range. A diversity of photonic devices based on ZnO micro/nanostructures, such as light emitting diodes, lasers, tunable filters, and optical sensors, have been achieved. Structurally, ZnO has three fast growth directions of [0001],[10$\bar{1}$0],and [2$\bar{1}\bar{1}$0], which benefits greatly the realization of many types of novel micro/nanostructures. Moreover, its unique structural properties also make the crystal growth behaviour of ZnO greatly sensitive to the growth conditions. This is why ZnO micro/nanostructures with different morphologies can be easily formed in the final products under the same preparation process.[11–13] However, the mechanistic reasons why a large amount of ZnO crystals with different morphologies can be formed under the same reaction conditions is rarely investigated. In addition, although numerous ZnO micro/nanostructures with different morphologies have been fabricated by a variety of chemical or physical methods, the micro/nanostructures used as FP microcavities have been realized only in 1D horizontal nanowires and nanobelts.[14,15]

In this work, we present the preparation of single crystalline ZnO multilayer hexagonal microplates (MHMs) and microtubes *via* a facile carbothermal reduction approach and show for the first time that such MHMs can be employed as vertical-FP microcavities. A thermodynamic effect is proposed to explain the

[a]*Key Laboratory of Materials for High-Power Laser, Shanghai Institute of Optics and Fine Mechanics, Chinese Academy of Science, Shanghai, 201800, China. E-mail: lzhang@siom.ac.cn*
[b]*State Key Laboratory of Surface Physics and Department of Physics, Fudan University, Shanghai, 200083, China. E-mail: zhanghai@fudan.edu.cn*
[c]*National Center of Theoretical Sciences at Taipei (Physics Division) and Department of Physics, National Taiwan University, Taipei, 10617, Taiwan*
[d]*National Laboratory for Infrared Physics, Shanghai Institute of Technical Physics, Chinese Academy of Sciences, Shanghai, 200438, China*

growth features of the microstructures with different morphologies. Fabry–Pérot modes (FPMs) were directly observed in the UV and visible spectral range at room temperature by using a spatially resolved spectroscopic technique. Finite-difference-time-domain (FDTD) simulations were performed to confirm that the resonant modes observed in the experiment are indeed FPMs. Furthermore, strong UV lasing was obtained from the ZnO MHMs, and the lasing behavior was investigated in detail by the temperature and excitation power dependence of a photoluminescence (PL) experiment. Compared with the conventional 1D nanowire/nanobelt FP cavities, these MHM vertical-FP microcavities have much less optical loss and provide efficient optical modulation, which are useful in the development of novel optical devices.

Experimental

Preparation

Single crystalline ZnO microstructures were prepared by an improved carbothermal reduction method. As distinct from the conventional chemical vapor deposition method, the present technique needs no catalysts, carrier gases, or vacuum conditions. The experimental setup is depicted in Fig. 1(a). Powders of ZnO and graphite were well mixed with a weight ratio of 1 : 1 and loaded into a small quartz boat as source material. A clean Si (111) substrate (2 × 1 cm) was placed on top of the quartz boat to collect the products. First, a quartz tube was inserted into a horizontal tube furnace and heated to 1050 °C. Then, the boat filled with the source material was pushed to the center of the quartz tube. After heating for about 5 min, the quartz boat was dragged out from the furnace quickly. A large amount of white products were formed on the surface of the Si substrate. Interestingly, three types of ZnO microstructures with different morphologies could be distinguished in three different regions from zone A to zone C of the Si substrate.

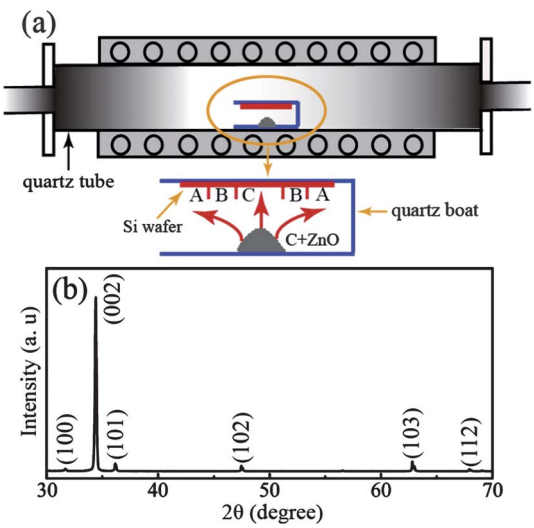

Fig. 1 (a) Schematic depiction of the experimental setup. The magnified sketch of the quartz boat shows the deposited position in the three zones A–C on the Si substrate. (b) XRD pattern of the obtained samples with different morphologies that were deposited on the whole Si substrate.

Characterization

The structure and morphology of the obtained products were characterized by scanning electron microscopy (SEM, Hitachi S-4800), transmission electron microscopy (TEM, JEOL JEM-2100F), and X-ray diffraction (XRD) (Bruker D8 ADVANCE). Optical studies of individual ZnO microplate were carried out using a confocal micro-photoluminescence system (JY LabRAM HR UV). A He-Cd laser at 325 nm and pulsed Nd:YAG laser at 355 nm were used as the excitation source. The excitation laser was focused by a microscope objective (40×) onto the microplate with a spot diameter of ~2 μm.

Results and discussion

Fig. 1(b) shows the XRD spectrum of the obtained products. All diffraction peaks can be assigned to the hexagonal wurtzite-type ZnO (JCPDS No. 65-3411). The predominant ZnO peak from (002) planes indicates that the microstructures were grown with *c*-axis orientation. No impurity peaks can be detected, which indicates that the samples are pure ZnO with the wurtzite structure.

The morphologies of the ZnO microstructures obtained at different regions from zone A to zone C on Si substrates were examined using SEM. Fig. 2(a) shows the SEM image of the ZnO microplates deposited in zone A with a spacing of about 0.5 mm. It can be seen that hexagonal-shaped microplates with length of side 3–5 μm were directly grown on the Si substrate. This kind of microplates was found in widespread existence in the A zone, far away from the source material. Fig. 2(b) shows the side view of a single ZnO microplate, revealing that the microplate has a distinctly layered structure with a flat and smooth top surface. Products collected from the intermediate zone of B (about 0.2 mm span) show microrod structures, and the typical morphology is shown in the SEM images in Fig. 2(c) and (d). The microrods have lengths in the range of 10–20 μm and an average diameter of about 5 μm. The detailed geometrical morphology is shown in Fig. 2(d), in which the microrod has a clean surface and a hexagonal cross section. On the side wall of the microrods, a few apparent growth stripes could be observed, which indicates that the microrods have a layered structure as well. Fig. 2(e) and (f) show the SEM images of microtubes with a high yield in zone C (spanning about 0.6 mm). Zone C is the nearest region to the source material. The lengths of the microtubes are 40–60 μm and the diameters are 2–4 μm. The high magnification SEM image of a single ZnO microtube is shown in Fig. 2(f). It can be clearly seen that the tube has a hexagonal cross section with regular and smooth outside surfaces. Based on the above SEM analyses, we can see that the observed morphologies of the microstructures depend on their distance with respect to the position of the source material.

All these three types of ZnO microstructures, microrods and microtubes have been studied as whispering gallery mode (WGM) microcavities in recent years.[16,17] As a new hierarchical microstructure, the ZnO MHM exhibits a regular hexagonal shape and smooth edges, which may be used as a good candidate for an optical microcavity. Therefore, we focus on the investigation of the ZnO MHMs. To get further information about the microstructure of the ZnO MHMs, TEM analysis was

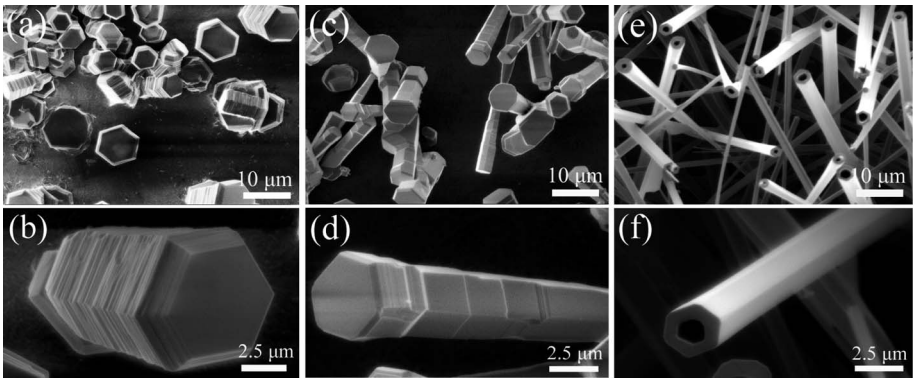

Fig. 2 SEM images of the synthesized ZnO microstructures collected from different zones. (a, b) MHMs in zone A; (c, d) microrods in zone B; (e, f) microtubes in zone C.

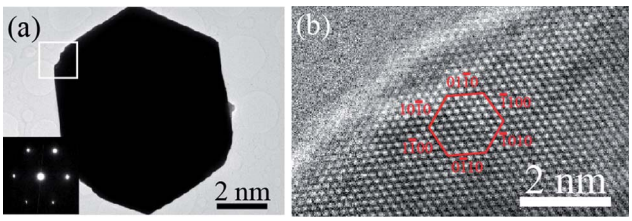

Fig. 3 (a) TEM image and the corresponding SAED pattern (inset) of an individual ZnO multilayer microplate. (b) HRTEM image corresponding to the rectangular region in (a).

performed. Fig. 3(a) shows the TEM image of one single ZnO MHM. The corresponding selected area electron diffraction (SAED) pattern (left inset in Fig. 3(a)) reveals a single diffraction pattern of the wurtzite ZnO phase. A high resolution TEM image taken from the rectangular region marked in Fig. 3(a) clearly displays surface steps and free of impurity.

The morphologies of the ZnO products depend strongly on the distance between the growth positions of the products and the source material. In other words, the concentration of the reactant is a crucial factor for the shape of the ZnO microstructures. In our system, graphite acts as a reducing agent, facilitating ZnO powder being reduced to Zn vapor at high temperature. The Zn atoms will then be oxidized in air, forming ZnO_x ($x \leq 1$) nanocrystals. For the reason why different microstructures can be formed in the same reaction process, the thermodynamic viewpoint should be taken into account. Note that ZnO/Zn is immiscible with Si, implying that the microstructures synthesized on the Si substrates will be affected by the interface energy. To minimize the interface energy, the growth preference of the ZnO nuclei will be altered with the change of the reactant concentration. If the concentration of Zn vapor is very high, excessive relative to oxygen, microtubes will be formed through an oxidation–sublimation process (zone C). The detailed formation mechanism has been discussed in our previous work.[16] The growth of ZnO microrods with obvious stripes and multilayer microplates suggests the layer-by-layer mode under a relatively low concentration of ZnO atoms (zone A and zone B). The ledge-flow and the two dimensional nucleation on the terrace are the two different modes in the layer-by-layer crystal growth.[18] Fig. 4 (a)–(d) show the schematic illustration of these two growth modes. The dominant factor that distinguishes the two growth modes is the relative concentration of ZnO on the growth position. In nature, the growth process is a competition between the horizontal surface diffusion and vertical growth of ZnO atoms to minimize the interface energy. Since the concentration of ZnO on the Si substrates was not uniform, ZnO crystals with a layered structure should be the result of the competition and equilibrium of these two growth modes. The typical SEM images of the samples obtained in different reaction regions are shown in Fig. 4 (e) and (f), which present a direct evidence of the two crystalline growth modes above.

Optical study of the ZnO MHMs is carried out under a confocal microphotoluminescence spectrometer, as schematically illustrated in Fig. 5(a). A 325 nm He-Cd laser was focused to a spot size ~2 μm through a microscope objective (40×) on a single MHM. A variable optical attenuator for the high power laser beam was used to adjust the excitation intensity. The PL

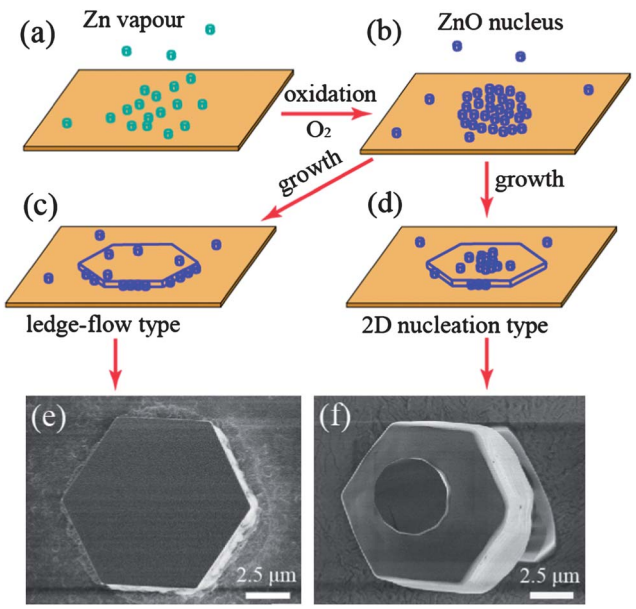

Fig. 4 (a–d) Schematic diagrams of the growth processes of the ledge-flow and the two dimensional nucleation on the terrace modes. (e,f) SEM images of two typical samples grown by the above two growth modes, respectively.

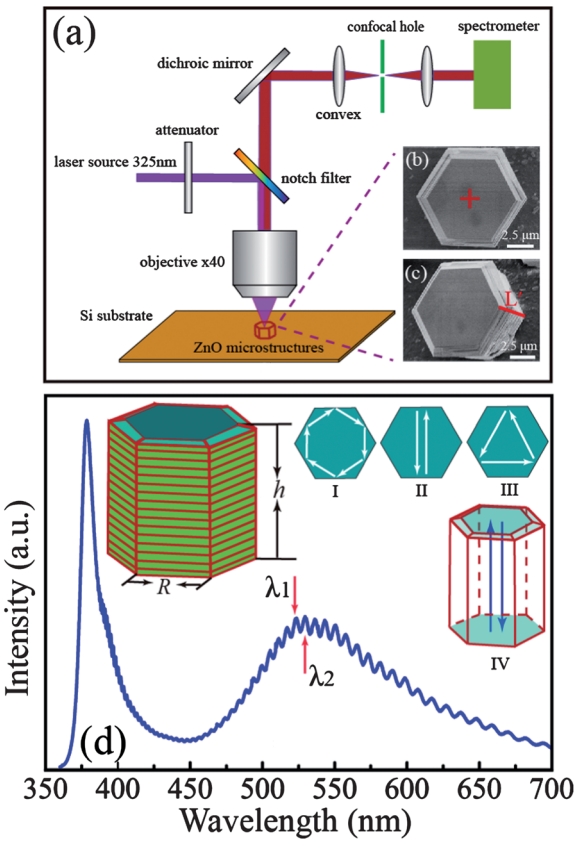

Fig. 5 (a) Schematic setup for the microphotoluminescence experiments of the microplates. (b–c) SEM images of the selected ZnO microplate used for the spectroscopic measurements, top-view and side-view (20° tilt), respectively. The focused laser spot is marked by a red cross. (d) PL spectrum from the individual ZnO microplate (Fig. 5(b)) shows a series of resonant cavity modes. The left inset of Fig. 5(d) is the side-view of a schematic microplate ZnO vertical-FP microcavity. The right insets show the diagrams of the four optical cavities: (I) WGM, (II) horizontal-FPM, (III) quasi-WGM, and (IV) vertical-FPM.

signal was collected by the same objective and recorded by a silicon CCD detector. In our experiments, a single ZnO MHM with regular hexagonal shape was selected for the investigation of the optical behavior. The top-view and side-view SEM images of this MHM are shown in Fig. 5(b) and (c), respectively. By focusing the laser spot at the center of the top facet of the selected microplate marked by a red cross as shown in Fig. 5(b), we observed a broad PL signal in the range of 360–700 nm, with clear modulations as shown in Fig. 5(d). These modulations correspond to the resonance of the optical modes. From the point of view of geometrical optics, four kinds of resonant cavity modes, WGMs (I), horizontal-FPMs (II), quasi-whispering gallery modes (quasi-WGMs), and vertical-FPMs, could be formed in such MHMs as shown in the right inset of Fig. 5(d). A light wave can travel around the cavity in a hexagonal closed path and in a triangular closed path due to the multiple total internal reflections at the interface between microplate and air, hence forming WGM and quasi-WGM, respectively. In the case of horizontal-FPM, light can travel back and forth between the two opposite edges of the microplates. In addition, vertical-FPMs can also be formed between the top and bottom parallel facets of the MHMs. In any of these resonant modes, the mode spacing $\Delta\lambda$ is given by[10]

$$\Delta\lambda = \frac{\lambda^2}{L\left(n - \lambda\frac{dn}{d\lambda}\right)} \quad (1)$$

where L is the path length of a round trip, n is the refractive index of the ZnO medium, and $dn/d\lambda$ is the dispersion relation. The mode spacing between two adjacent cavity modes (λ_1 = 523.3 nm, λ_2 = 529.6 nm) is 6.3 nm according to the measured PL spectrum (Fig. 5(a)). Using the dispersion of ZnO,[15] the corresponding refractive index is $n = 2.04$, and $\lambda dn/d\lambda$ is about −0.593 at the wavelength of ~523.3 nm. The path length of a round trip is calculated to be about 16.56 μm. The side length R of the MHM used for the PL measurement is about 5.26 μm as determined by the SEM image. If the resonant modes were WGMs, the deduced $L = 3\sqrt{3}R$ is about 27.33 μm. If the resonant modes originated from the horizontal-FP cavity, the deduced $L = 2\sqrt{3}R$ is about 18.22 μm. If the resonant modes were quasi-WGMs, it can be deduced that the path length $L = 4.5R$ is about 23.67 μm. Obviously, the above calculated path lengths are all much larger than the observed value in our experiment, which indicates that the resonant modes are not from the WGM, horizontal-FPM or quasi-WGM cavity. For the vertical-FPMs, L is two times as long as the height of the MHM. From Fig. 5(c), we can determine the L' is about 2.82 μm, and the tilted angle of the microplate is 20°. The height of the selected MHM can be calculated as ~8.25 μm, which is consistent with the height of the MHM (8.28 μm) obtained in the above theoretical analysis basing on the measured resonant modes. Thus, one can attribute the measured resonant modes to the effect of the vertical-FPM type cavity. Such MHM vertical-FP cavities need not to be removed from their growth substrate, which preserved their structure and geometric configuration. This not only avoids the adverse effects faced by the conventional 1D horizontal FP microcavities but also is conducive to obtain the accurately unperturbed nature of ZnO optical interferences. This will have potential applications in the development of novel optical devices.

To identify the nature of the resonant modes observed experimentally, we employed the FDTD method[19] to study the optical modes in such ZnO MHM cavities. From the point of view of FP resonant mechanism, our MHM microcavity is equivalent to the hexagonal microrod microcavity, with the top and bottom parallel facets acting as reflecting mirrors. Limited by the computation resources, in our FDTD simulations, we studied a single ZnO hexagonal microcavity (Fig. 6(d)) with radius 2.5 μm smaller than that of the real sample. The height of the ZnO microcavity was fixed as 8.28 μm, consistent with the experimental data. In our simulations, we shined a plane wave normally on the top surface of the microcavity, and calculated the scattering spectra. To ensure a fast convergence in the calculations, we added a tiny loss to the permittivity of ZnO. As the resonant modes formed within the UV frequency region are too dense to resolve, we focused on those appearing in the visible frequency region. From the calculated backward reflection spectrum depicted in Fig. 6(b), we found a series of resonance peaks whose positions match perfectly with the experimental

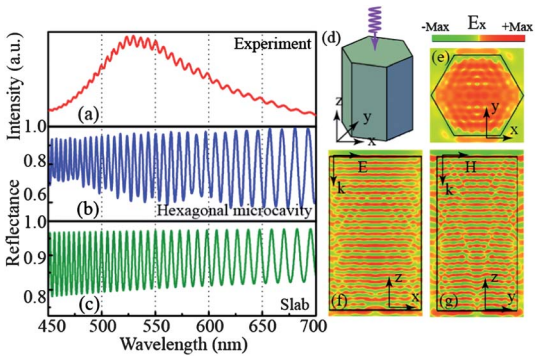

Fig. 6 (a) Measured photoluminescence spectrum from an individual ZnO microplate microcavity in the visible frequency region. Backward reflection spectra for a single ZnO hexagonal microcavity (b) and a slab model (c) calculated by FDTD simulations under a normal illumination of plane wave. (d) Schematic diagram of the simulated ZnO hexagonal microcavity. Simulated electric field intensity distribution of the simulated hexagonal microcavity at $\lambda = 626$ nm along different symmetric planes (e), (f) and (g).

results (Fig. 6(a)). Such an excellent agreement is the direct proof that the experimentally observed optical modes are indeed the vertical-FPMs. Although the simulated structure has a smaller lateral size than the experimental sample, such a difference will not affect the final conclusions since the vertical-FPMs do not depend on the lateral size of the microcavity. To gain a better understanding on the simulation results, we performed another simulation with the microcavity replaced by a flat dielectric slab with refractive index and height being the same as those of the ZnO microcavity. The calculated results are depicted in Fig. 6(c). The slab model yields a series of resonant modes, which also match well with the experimental results. Such agreement further confirms that the observed resonance modes in the complicated structure must be the FP modes since the slab model cannot support any other types of optical mode. As an illustration, we depicted in Fig. 6(e)–(g) the electric field distributions inside the measured microcavity, calculated at the wavelength 626 nm (corresponding to one resonant peak). Fig. 6(e) shows that the optical energy is mainly confined in the centre of the microplate as FP resonators. The mode profiles along the ZnO hexagonal microcavity (Fig. 6(f) and (g)) clearly show a standing wave formed between the top and bottom facets of the multilayer microplate, being the features of a typical FP-type resonance.

The PL spectra of ZnO MHMs with different heights (h = 3.38, 7.97, 9.86 μm) were measured to investigate the relationship between the vertical-FP-type resonance modes and the sizes of the MHM microcavities. As shown in Fig. 7, the PL signals in UV and visible spectra range are clearly modulated by varying the size of the cavity. Theoretical calculation indicates that the reflectance of visible light at the ZnO/air boundary never exceeded 13%.[20] It is inspiring that a series of FP resonant modes can be clearly identified in such a vertical microcavity with a shot effective length. The number of FP resonance modes increases distinctly with increasing height of the cavity. From eqn (1), we can see that the mode spacing is inversely proportional to the effective length of the cavity. As shown by the measured results, the mode spacing expands with decreasing height of the cavity, which is consistent with the description of the mode spacing

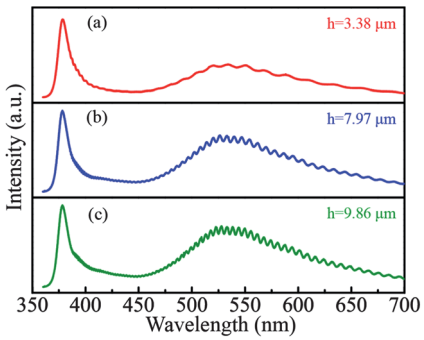

Fig. 7 Modulated PL spectra collected at the center of the top facet of three ZnO MHMs with different heights.

equation. In addition, the width of the mode peak significantly decreases as the MHM height enlarges, indicating that the increase of the cavity height can improve the mode quality.

As shown in Fig. 5, the PL from the ZnO MHM consists of two emission bands, a UV emission and a broad visible emission. The origin of the visible emission is mainly attributed to impurities and/or point defects.[21] The UV emission at about 385 nm is the band-edge emission resulting from exciton transition and their photo replicas.[22] It is this UV emission band that allows us to systematically investigate the lasing action in such MHM vertical-FP microcavity. Fig. 8(a) shows the excitation power-dependent PL spectra of the above-mentioned ZnO MHM measured at 10 K. The maximum of the UV emission band, compared with those taken at room temperature, has an obvious blue shift and is located at ~375 nm. When the excitation power was increased to a threshold of ~0.4 μW, some discrete laser lines were generated abruptly on the spontaneous emission band. By further increasing the excitation level, the intensity of the laser lines exponentially increased and new peaks appeared on the lower-energy side. This clearly indicates that lasing occurs in the ZnO MHM. To further investigate the UV lasing property of the ZnO MHM, the temperature-dependent PL spectra measured between 10 and 190 K with a fixed excitation power of ~3.2 μW are shown in Fig. 8(b). With the increase of the temperature, the intensities of all emissions are decreased, and the peak position shows a significant red-shift. The decrease in intensity is due to the result of the thermalization.[23] The average kinetic energy and momentum of excitons become large with increasing temperature. Those excitons with certain kinetic

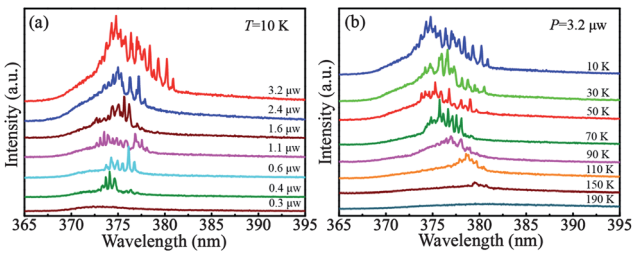

Fig. 8 The emission spectra of one single ZnO microplate: (a) excitation power-dependent PL spectra measured at 10 K, (b) temperature-dependent PL spectra in the range of 10–190 K under a fixed excitation power of ~3.2 μW.

energies would be easily trapped by surface states or defect centers, and then enter the nonradiative recombination channels. Thus, the number of the excitons close to the center of the Brillouin zone decreases, resulting in the reduction of the efficiency of the radiation recombination. That is why the numbers of lasing peaks decreases very quickly with increasing temperature and cannot be generated at temperatures higher than 190 K. The red-shift with increasing temperature can be attributed to the temperature induced lattice dilatation and electron-lattice interaction.[24] Our results provide directly a physical picture of the temperature- and excitation power-dependent FPM lasing, which is important for further understanding the FPM lasing action, aiming at the development of novel UV microlasers.

Conclusion

In summary, single crystalline ZnO MHMs and microtubes were prepared through a facile carbothermal reduction method, and the MHM was first studied as an efficient vertical-FP microcavity. The growth mechanism and shape diversity were analyzed and explained by a proposed thermodynamic model. By using a spatially resolved spectroscopic technique, FPMs and UV lasing were directly observed from the ZnO MHMs, which agrees well with the results from FDTD simulations. Furthermore, the lasing behavior was investigated in detail by the temperature and excitation power dependence of PL experiments. The experimental and theoretical analysis demonstrated that such a MHM vertical-FP microcavity can be a good candidate for the development of novel optical and lasing devices.

Acknowledgements

This work was supported financially by the NSFC (61108059, 50802103, 51072207, 60725417, 60990321, 61178007), the program of the excellent academic leaders of Shanghai (10XD1404600), MOE of China (B06011), Shanghai Science and Technology Committee (08dj1400302), STCSM Nano Project, (11nm 0502400) and the 100-Talent Program of Chinese Academy of Sciences and the starting grant of SIOM (1108221-JR0).

Notes and References

1 B. Min, E. Ostby, V. Sorger, E. U. Avila, L. Yang, X. Zhang and K. Vahala, *Nature*, 2009, **457**, 455.
2 F. Qian, Y. Li, S. Gradecak, H.-G. Park, Y. Dong, Y. Ding, Z. L. Wang and C. M. Lieber, *Nat. Mater.*, 2008, **7**, 701.
3 R. Chen, B. Ling, X. W. Sun and H. D. Sun, *Adv. Mater.*, 2011, **23**, 2199.
4 S. Chu, G. P. Wang, W. H. Zhou, Y. Q. Lin, L. Chernyak, J. Z. Zhao, J. Y. Kong, L. Li, J. J. Ren and J. L. Liu, *Nat. Nanotechnol.*, 2011, **7**, 701.
5 X. L. Xu, F. S. F. Brossard, D. A. Williams, D. P. Collins, M. J. Holmes, R. A. Talylor and X. T. Zhang, *Appl. Phys. Lett.*, 2009, **94**, 231103.
6 J. C. Johnson, H. J. Choi, K. P. Knutsen, R. D. Schaller, P. D. Yang and R. J. Saykally, *Nat. Mater.*, 2002, **1**, 106.
7 R. M. Ma, X. L. Wei, L. Dai, S. F. Liu, T. Chen, S. Yue, Z. Li, Q. Chen and G. G. Qin, *Nano Lett.*, 2009, **9**, 2697.
8 Y. Ding, J. Motohisa, B. Hua, S. Hara and T. Fukui, *Nano Lett.*, 2007, **7**, 3598.
9 C. Zhang, C. L. Zou, Y. L. Yan, R. Hao, F. W. Sun, Z. F. Han, Y. S. Zhao and J. N. Yao, *J. Am. Chem. Soc.*, 2011, **133**, 7276.
10 D. J. Gargas, M. E. Toimil-Molares and P. D. Yang, *J. Am. Chem. Soc.*, 2009, **131**, 2125.
11 X. Liao and X. Zhang, *J. Phys. Chem. C*, 2007, **111**, 9081.
12 Z. W. Pan, J. D. Budai, Z. R. Dai, W. J. Liu, M. P. Paranthaman and S. Dai, *Adv. Mater.*, 2009, **21**, 890.
13 M. R. Shi, F. Xu, K. Yu, Z. Q. Zhu and J. H. Fang, *J. Phys. Chem. C*, 2007, **111**, 16267.
14 M. A. Zimmler, J. M. Bao, F. Capasso, S. Müller and C. Ronning, *Appl. Phys. Lett.*, 2008, **93**, 051101.
15 S. Rühle, L. K. van Vugt, H. Y. Li, N. A. Keizer, L. Kuipers and D. Vanmaekelbergh, *Nano Lett.*, 2008, **8**, 119.
16 H. X. Dong, Z. H. Chen, L. X. Sun, W. Xie, H. Hoe Tan, J. Lu, C. Jagadish and X. C. Shen, *J. Mater. Chem.*, 2010, **20**, 5510.
17 L. X. Sun, Z. H. Chen, Q. J. Ren, K. Yu, L. H. Bai, W. H. Zhou, H. Xiong, Z. Q. Zhu and X. C. Shen, *Phys. Rev. Lett.*, 2008, **100**, 156403.
18 Y. H. Yang, B. Wang and G. W. Yang, *Nanotech.*, 2006, **17**, 5556.
19 *EastFDTD 2.0*, Dongjun Technology, China, 2010.
20 J. Z. Liu, S. Lee, Y. H. Ahn, J. Y. Park, K. H. Koh and K. H. Park, *Appl. Phys. Lett.*, 2008, **92**, 263102.
21 M. Willander, L. L. Yang, A. Wadeasa, S. U. Ali, M. H. Aaif, Q. X. Zhao and O. Nur, *J. Mater. Chem.*, 2009, **19**, 1006.
22 X. X. Zhang, D. F. Liu, L. H. Zhang, W. L. Li, M. Gao, W. J. Ma, Y. Ren, Q. S. Zeng, Z. Q. Niu, W. Y. Zhou and S. S. Xie, *J. Mater. Chem.*, 2009, **19**, 962.
23 W. Shan, W. Walukiewicz, J. W. Ager III, K. M. Yu, H. B. Yuan, H. P. Xin and G. Cantwell, *Appl. Phys. Lett.*, 2005, **86**, 191911.
24 B. Q. Cao, W. P. Cai and H. B. Zeng, *Appl. Phys. Lett.*, 2006, **88**, 161101.

